Archaeological Prospection
Archaeol. Prospect. **15**, 93–112 (2008)
Published online 6 May 2008 in Wiley InterScience
(www.interscience.wiley.com) DOI: 10.1002/arp.327

Three-dimensional, Multi-offset Ground-penetrating Radar Imaging of Archaeological Targets

ADAM D. BOOTH[1,4]*, NEIL T. LINFORD[2], ROGER A. CLARK[3] AND TAVI MURRAY[1]

[1] *Glaciology Group, Department of Geography, School of the Environment and Society, Swansea University, Singleton Park, Swansea, SA2 8PP, UK*
[2] *Geophysics Team, English Heritage, Fort Cumberland, Eastney, Portsmouth, PO4 9LD, UK*
[3] *School of Earth and Environment, Faculty of Environment, University of Leeds, Woodhouse Lane, Leeds, LS2 9JT, UK*
[4] *School of Geography, Faculty of Environment, University of Leeds, Woodhouse Lane, Leeds, LS2 9JT, UK*

ABSTRACT The efficacy of ground penetrating radar (GPR) methods is inhibited when surveying over a target that is structurally complex and/or hosted within attenuative media. Recent research has documented the ability of certain seismic methods to improve imaging using GPR. For imaging complex targets, three-dimensional acquisition and migration methods are applied. For attenuative sites, signal-to-noise ratio (SNR) may be boosted on acquisition of multi-offset data. We present results from an integrated three-dimensional multi-offset survey over a Romano-British villa at Groundwell Ridge, near Swindon, UK. Data were acquired within a grid of dimension 21 m $\times$ 14 m, using a single-channel PulseEKKO GPR system equipped with common-offset (CO) 450 MHz antennas. To satisfy criteria for three-dimensional migration, the sample density over the grid was 0.05 $\times$ 0.05 m^2. A smaller grid of three-dimensional multi-offset data was acquired, with fold-of-cover 2200%, targeting a low SNR section of data. The spatial resolution and SNR in the resulting images of the target are greatly improved compared with data acquired using a more conventional survey method. However, this improvement may not be justified by the greatly increased (some 10 times) fieldwork effort required to obtain three-dimensional multi-offset data. We therefore investigate a means of improving the efficiency of three-dimensional GPR surveying by applying a simple trace interpolation method to recover three-dimensional acquisition criteria. This trial suggests that, at this site, three-dimensional data can be simulated from a grid of *pseudo*-three-dimensional data, sampled at 0.05 $\times$ 0.25 m^2. In this way, high quality images of an archaeological target can be obtained with minimal increase to survey effort. We hope that, on the basis of this work, three-dimensional and multi-offset acquisitions will be more readily considered for archaeological GPR investigations. Copyright © 2008 John Wiley & Sons, Ltd.

Key words: ground penetrating radar; three-dimensional migration; multi-offset; resolution; signal-to-noise ratio; imaging

Introduction

Ground-penetrating radar (GPR) techniques are widely applied in archaeological investigations

* Correspondence to: A. D. Booth, Glaciology Group, Department of Geography, School of the Environment and Society, Swansea University, Singleton Park, Swansea, SA2 8PP, UK. E-mail: a.d.booth99@leeds.ac.uk

Received: 13 July 2007
Accepted 4 January 2008

and, in many cases, provide faithful, high-resolution images of subsurface targets. In spite of many successful demonstrations of the GPR method, its efficacy is inhibited where low signal amplitudes are returned to the GPR system with respect to some ambient noise level, or where a survey is conducted over a target that is structurally complex (e.g. Linford and Linford, 2004; Grasmueck *et al*., 2004, 2005). Low signal amplitudes may result where a target is located in electrically conductive, and therefore attenuative, media (e.g. Olhoeft, 1996; Linford and Linford, 2004) or where that target has a low physical contrast with its host (e.g. Witten *et al*., 2000; Pipan *et al*., 2005). Surveying over a complex subsurface structure may produce radargrams which are difficult to interpret accurately, due to reflections originating from outside of the plane of the profile; these reflections cannot be correctly migrated using conventional two-dimensional migration strategies (Leckebusch, 2000; Yilmaz, 2001).

In recent years, increasingly sophisticated acquisition and processing techniques have been imported from reflection seismology to the GPR setting (e.g. Fisher *et al*., 1992; Pipan *et al*., 1999, 2005; Grasmueck *et al*., 2005; Berard and Maillol, in press) with the aim of overcoming these issues. In order to improve the signal-to-noise ratio (SNR) in a dataset, GPR data may be acquired using the multi-offset (MO) method (e.g. Fisher *et al*., 1992; Pipan *et al*., 1999, 2005). To improve spatial resolution over a subsurface with complex reflectivity, GPR data should be acquired according to full-resolution criteria (Grasmueck *et al*., 2005) to mitigate spatial aliasing and facilitate three-dimensional migration. Acquisition of such advanced datasets is inefficient with current GPR technology, compared with conventional GPR practice, hence their use is rare; rarer still is the integrated acquisition of data that are both three-dimensional and multi-offset. We therefore present in this paper the results from an integrated multi-offset, full-resolution three-dimensional GPR acquisition over buried Romano-British building remains at Groundwell Ridge, near Swindon, UK (Linford and Linford, 2004). Although image quality is greatly improved by application of multi-offset and full-resolution techniques, it is questionable whether that improvement justifies the greatly increased acquisition effort. We therefore also investigate a means of improving the efficiency of full-resolution surveying by use of a trace interpolation scheme to increase sample density from a more conventional acquisition strategy to full-resolution criteria. As a result of this work, it is hoped that three-dimensional and/or multi-offset GPR acquisitions will be more readily considered for image enhancement.

Full-resolution, three-dimensional ground-penetrating radar surveying

Three-dimensional methods were developed by the seismic industry to improve imaging around complex, often steeply orientated, structures (such as the flanks of salt structures around which may be located significant hydrocarbon reserves; Yilmaz, 2001). In many respects, archaeological remains are equally complex; walls of buildings are originally vertical and, furthermore, they may exhibit abrupt changes in direction as the corner of the building is reached (e.g. the rectilinear ground plan of many Roman buildings; e.g. Gaffney *et al*., 2000; Linford and Linford, 2004). Grasmueck *et al*. (2005) demonstrate the application of three-dimensional GPR methods to imaging fractures in carbonate strata but suggest that, due to the potential complexity of targets, the technique would also be useful for archaeological imaging.

For several years, archaeological geophysicists have appreciated that a better understanding of the spatial extent of targets is obtained from a grid, rather than a profile, of GPR data; acquisition of grids of GPR data is commonplace (e.g. Leckebusch, 2003; Gaffney *et al*., 2004; Gustaffson and Alkarp, 2007). However, the spatial sampling density of the majority of GPR grids is insufficient for three-dimensional migration (e.g. Whiting *et al*., 2001; Linford and Linford, 2004; Pipan *et al*., 2005; Ranieri *et al*., 2005; Pomfret, 2006) given that they do not fulfil established full-resolution sampling criteria. Grasmueck *et al*. (2005) state that, for a grid of common offset (CO) GPR data, three-dimensional sampling criteria are fulfilled if the maximum spatial sampling interval, Δx_{max}, along and

DOI: 10.1002/arp

between profiles does not exceed ¼ of the apparent wavelength, λ_{app}, of the GPR energy, i.e.

$$\Delta x_{max} < \frac{\lambda_{app}}{4} = \frac{v}{4f \sin \alpha}, \quad (1)$$

where v is the near-surface propagation velocity of the GPR wavelet, f is the dominant frequency of energy and α is the angle, to the vertical, of energy arriving at the surface. To ensure that all dip components of the GPR wavefield are faithfully sampled it is prudent to assume $\alpha = 90^\circ$; as such, $\sin(\alpha) = 1$ and Δx_{max} can be constrained in terms of velocity and frequency alone. In practice, however, Grasmueck *et al.* (2005) state that $\alpha = 60^\circ$ is sufficient for most commercial GPR systems, as significant energy is not radiated or received at angles greater than this. Where the spatial sampling criteria of a survey do not satisfy the above criteria, the recorded wavefield is described as *spatially aliased*.

A major advantage of the GPR technique is that the short wavelength of GPR energy offers high-resolution imaging of subsurface structure. However, this short wavelength implies that full-resolution survey criteria will be somewhat daunting. Substituting values of $f = 500$ MHz, $v = 0.08$ m ns^{-1} (representative of conditions found on many archaeological sites in the UK) and $\alpha = 60^\circ$ into Equation 1 predicts that the maximum spatial sampling interval in the GPR survey should be less than 0·054 m. Although this is typical of the sampling interval along profiles (i.e. *in-line* sampling between individual traces), it is much smaller than the typical lateral separation between profiles (i.e. *cross-line* sampling). As such, typical three-dimensional GPR grids are spatially aliased in the cross-line direction and are more appropriately described as *pseudo*-three-dimensional.

Migration of data, where applied effectively, can provide a superior image of subsurfaces; the process returns energy to its true point of origin in the subsurface and improves the lateral resolution of the GPR wavelet (e.g. Lindsey, 1989; Leckebusch, 2000; Leucci, 2002; Gustafsson and Alkarp, 2007). When applied in a conventional two-dimensional sense, migration is only correctly applied to energy that originates from within the plane of the survey line; furthermore, spatial resolution is only improved in the in-line direction (Lindsey, 1989). Serious migration artefacts can be produced from application of two-dimensional migration to out-of-plane energy since it is repositioned incorrectly and, as a result, the interpretation may be incorrect. Effective three-dimensional migration is able to process out-of-plane energy, and also improves spatial resolution in both in-line and cross-line directions. However, three-dimensional migration is only robustly applied where the spatial sampling criteria of a wavefield fulfils full-resolution criteria. Since grids of GPR data are typically spatially aliased in the cross-line direction, three-dimensional migration cannot be robustly applied to these conventional pseudo-three-dimensional grids. Where spatial sampling criteria are satisfied, three-dimensional migration methods are still not necessarily applied; Gustaffsson and Alkarp (2007) describe an archaeological GPR acquisition that satisfies full-resolution criteria, but migrate data only with a two-dimensional algorithm. We therefore investigate the improvement to the image of an archaeological target that results from application of three-dimensional migration methods to full-resolution GPR data.

Multi-offset ground-penetrating radar surveying

The multi-offset method is a well-rehearsed technique developed by the seismic community with the aim of improving SNR. The conventional common-offset method of acquiring GPR data fixes the separation between transmitting and receiving antennae, Tx and Rx respectively, at all survey locations. With this antenna configuration, subsurface reflection points are imaged once only by a raypath with a single geometry; as such, common-offset acquisitions yield *single-fold* (SF) data. In the multi-offset method, the separation between Tx and Rx is incrementally increased at each survey location. In a common mid-point (CMP) acquisition, antennae are offset about some fixed surface mid-point between Tx and Rx. Where a large-scale multi-offset survey is planned, data are acquired more efficiently using a common-source

DOI: 10.1002/arp

(CS) antenna configuration (e.g. Berard and Maillol, in press); the position of Tx is fixed and the offset to Rx is incrementally increased. Both multi-offset configurations yield *multi-fold* (MF) data, given that subsurface reflection points are imaged several times by numerous raypaths. Schematic common-offset and common-source acquisitions are shown in Figure 1.

Compared with a common-offset dataset, a greater range of processing algorithms are available for application to multi-offset data; there is, therefore, greater potential to improve SNR in a multi-offset dataset. One such algorithm is horizontal stacking of CMP gathers (Mayne, 1962), in which reflection travel-times in a CMP gather are corrected for normal-moveout (NMO) and amplitudes summed across the offset range; where a CMP gather contains n traces, application of horizontal stacking improves SNR by a factor of approximately $n^{1/2}$ (Sheriff and Geldart,

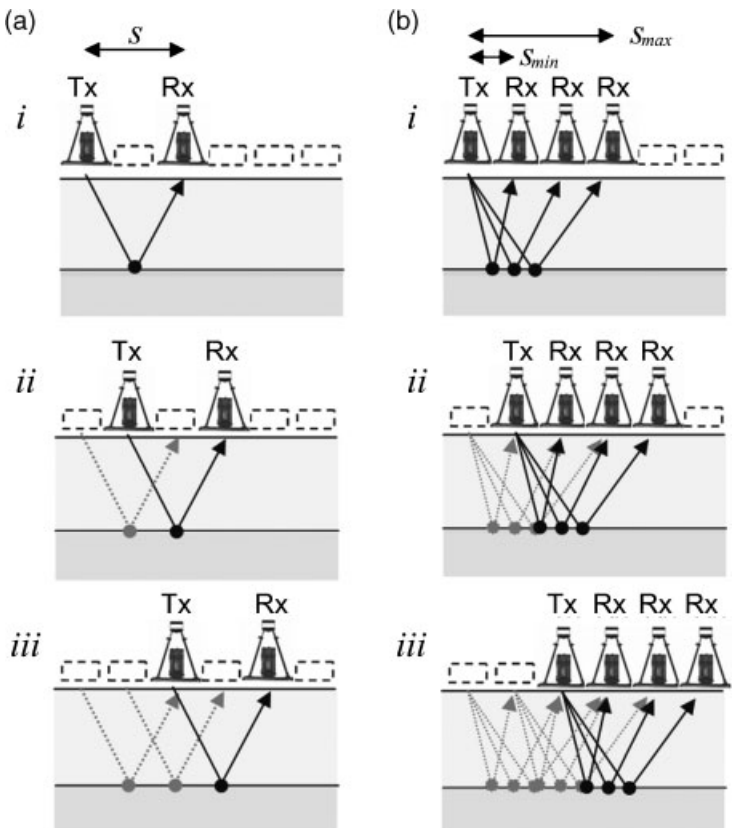

Figure 1. Schematic common-offset and common-source acquisitions at 3 surface locations, *i*, *ii* and *iii*, above a single subsurface interface. Solid arrows represent reflected raypaths for the current Tx-Rx positions, dashed arrows for previous acquisitions; similarly, black and grey circles show reflection points for current and previous Tx-Rx positions. Dashed boxes show unoccupied antenna positions. a) common-offset acquisition. At each location, Tx-Rx offset is fixed at some constant distance, *s*. Reflection points are imaged once only by a raypath with a single geometry. b) common-source acquisition. Tx position is fixed at each survey location and the offset to Rx is increased, incrementally, through a range s_{min} to s_{max}. The density of raypaths in the ground is greatly increased, and reflection points are imaged multiple times.

DOI: 10.1002/arp

1999). Common mid-point gathers are often used to obtain isolated velocity models (Sambuelli *et al*., 1999), but for a profile of multi-offset data a velocity model may be defined at every CMP location (e.g. Neidell and Taner, 1971). Where this velocity model is used as an input to a migration algorithm, the migration would be expected to perform more accurately than if a constant velocity subsurface was assumed. As a further means of improving SNR, an extended range of processing algorithms are available for multi-offset data for the suppression of coherent noise energy (e.g. where data are contaminated with reflected, refracted and/or diffracted airwaves; Bano *et al*., 1999; Pipan *et al*., 1999).

With current GPR instrumentation, field acquisition of multi-offset data is inefficient compared with common-offset data; however, several studies have shown considerable improvement where multi-offset data are compared with common-offset. Although initially demonstrated for geological imaging (Fisher *et al*., 1992), numerous multi-offset GPR surveys of archaeological targets have been conducted (Pipan *et al*., 1999, 2004, 2005; Berard and Maillol, 2007); multi-offset methods are particularly useful for archaeological imaging, as targets often have low physical contrasts with host media given that natural processes of site formation often result in a gradational, rather than discrete, transition in dielectric properties (Pipan *et al*., 2005). In this paper, we present results from acquisition of a full-resolution three-dimensional grid of multi-offset data. By integrating these methods, we hope to obtain an archaeological image that has both improved spatial resolution and elevated SNR compared with conventional GPR acquisitions.

Romano-British archaeology at Groundwell Ridge

Remains of Roman buildings were discovered at the Groundwell Ridge site (NGR: SU 141 894) in 1996, during construction of a housing estate. These remains are hosted within shallow, well-drained, clayey soils of the Sherbourne (343d) Association (Soil Survey of England and Wales, 1983). English Heritage (EH) geophysicists conducted magnetic and earth resistance surveys, from which the presence of a significant Romano-British settlement was inferred (Linford, 1999; Linford and Martin, 2002). These data were used to target a GPR grid, of dimension 3.6 ha, including the remains of a substantial (15 m × 20 m) building towards the southern edge of the settlement (Linford and Linford, 2004). The GPR data were acquired in July 2002 using a pulseEKKO1000 system, equipped with antennae of centre-frequency 450 MHz; the sample density of the EH grid was 0.05 m in the in-line direction, and 0.50 m in the cross-line direction. Figure 2 shows a representative GPR amplitude time-slice, together with a combined graphical summary of significant anomalies recorded in these data (Linford and Linford, 2004).

The time-slice in Figure 2a is centred on a two-way travel time (TWTT) of 19 ns, with the envelope of trace amplitudes summed over 18–20 ns to boost SNR. Using a CMP-derived velocity of 0.065 m ns^{-1}, this TWTT corresponds to a depth of 0.65 to 0.72 m. Data were processed using conventional dewow and bandpass filters and amplitude recovery methods; a two-dimensional migration was then applied in the in-line direction. Signal strength over this site is generally good, and strong reflections are identified over most of the survey area. However, SNR is somewhat reduced in the centre and towards the northeast corner of the building; reduced SNR could be attributed to a local increase in clay content (unlikely), lower physical contrast between local target and host, and/or increased GPR scattering due to a local increase in structural complexity.

The geophysical interpretation in Figure 2b shows the Groundwell Ridge target to have the characteristic rectilinear ground plan typical of a Romano-British villa (Wilson, 2002; Gaffney *et al*., 2004), comprising central rooms flanked by corridor wings. Although the exterior wall of the building is well-defined, low-SNR leads to a cautious interpretation of some of the internal structure. Numerous track-ways and enclosures are also observed, together with the response to a modern ferrous pipe which intersects the north-western corner of the building, and an anomaly over the eastern exterior wall that is attributed to the presence of a modern footpath.

DOI: 10.1002/arp

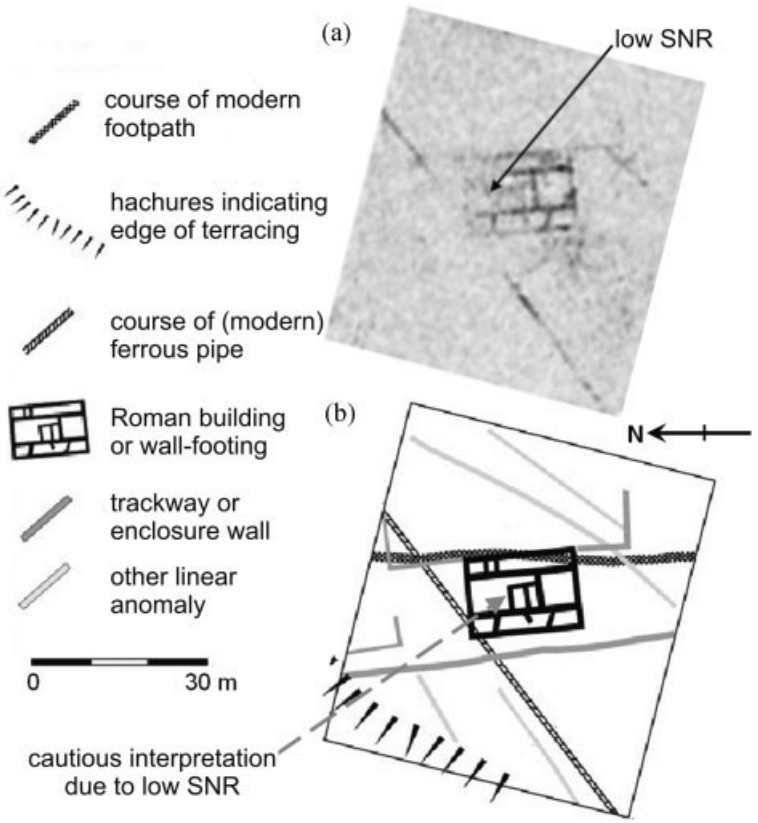

Figure 2. Representative GPR time-slice and combined geophysical interpretation from geophysical surveys as conducted by English Heritage during 2002 (Linford and Linford, 2004). a) GPR time-slice, greyscale display, originating from TWTT of 18–20 ns (0.65–0.72 m depth). b) Interpretation, combining inferences from magnetometer and earth resistance surveys. In addition to the clear Roman wall footing, other features (e.g. track-ways and enclosures, and the course of a modern footpath and ferrous pipe) are also identified.

The GPR image from the 2002 survey would be sufficient for the planning of archaeological excavations but a more complete interpretation over the whole area of the villa would be difficult given the variable data quality. If the spatial variability in SNR is due to local structural complexity, an improved image may be obtained on application of three-dimensional migration. However, the sampling interval between profiles in the EH grid was too coarse; cross-lines are spatially aliased, hence three-dimensional migration cannot be robustly applied. If low-contrast targets are the cause of poor SNR, acquisition of multi-offset data may boost signal strength such that reflectivity may be more rigorously interpreted. We therefore targeted this villa for trialling integrated acquisition of full-resolution three-dimensional multi-offset GPR data, with the aim of boosting the SNR and improving the interpretation of the internal structure.

Three-dimensional, multi-offset ground-penetrating radar acquisition

Full-resolution grids of three-dimensional common-offset and three-dimensional multi-offset GPR data were acquired at the Groundwell Ridge site in spring 2006; locations of those grids is shown in Figure 3. Similar to the EH survey, data were acquired using a Sensors and Software pulseEKKO1000 system equipped with 450 MHz antennae. A grid of dimension 21 m × 14 m was established over the northern half of the building using a Trimble kinematic differential global positioning system, based on the results of the

DOI: 10.1002/arp

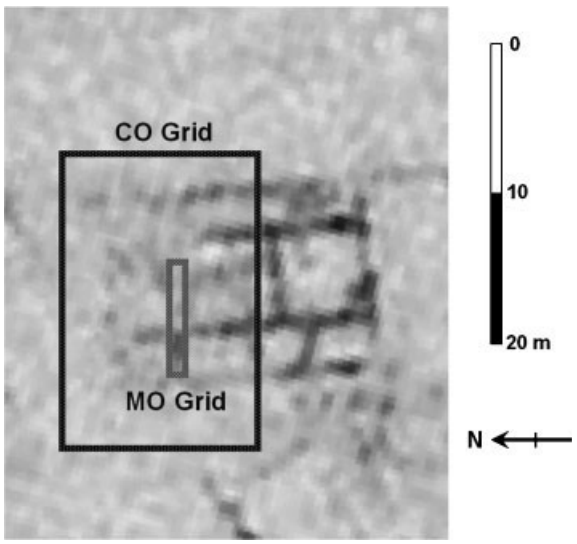

Figure 3. Location of the three-dimensional common-offset (heavy outline) and three-dimensional multi-offset (lighter, internal, outline) grids for the GPR survey of spring 2006, with respect to the representative time-slice from Figure 2. The three-dimensional common-offset grid ($21 \times 14\,m^2$ area) targets the northern half of the building. The three-dimensional multi-offset survey ($8 \times 1.35\,m^2$ area) targets structures over the possible location of an interior wall to the east of the grid.

previous geophysical survey. Representative CMP data were acquired at the known location of an external wall and used in Equation 1 to inform Δx_{max}. The dominant frequency of reflected energy was approximately 340 MHz and velocity was measured, using a semblance analysis (Neidell and Taner, 1971), slightly faster than in the previous acquisition at $0.069\,m\,ns^{-1}$; these CMP data are shown in Figure 4. With the assumption of vertical dip, Equation 1 predicts that full-resolution criteria are satisfied where Δx_{max} is less than 0.051 m; if the 60° recommendation of Grasmueck *et al*. (2005) is considered, the maximum spatial sampling interval should be 0.068 m. We therefore fixed Δx_{max} to 0.05 m in all grids.

The northern half of the building was surveyed using three-dimensional common-offset methods. Profiles were orientated east–west, with the fixed offset between Tx and Rx set at 0.2 m. This grid, with sample density $0.05 \times 0.05\,m^2$, took nine days to complete and comprises 117 739 individual GPR traces (281 in-lines, 419 cross-lines), with vertical stacking set to 16. Although the use of an odometer wheel would have improved acquisition efficiency, we followed the example of Pipan *et al*. (1999) and used antennae in static mode to ensure good ground coupling.

On completion of the common-offset grid, we identified the lowest SNR region of the dataset and targeted this area with a three-dimensional multi-offset grid of dimension $8\,m \times 1.35\,m$. This location coincided with the lowest SNR region of the 2002 acquisition, where a cautious interpretation of an east-west trending internal wall had been made. By boosting SNR at this location, we intend to test the fidelity of this interpretation. A common-source gather was acquired every 0·05 m along east–west profiles, again separated by 0.05 m. In each common-source gather, the position of Tx is fixed and the offset to Rx is increased, in increments of 0.05 m, through a distance range of 0.2 to 2.35 m (constrained using the methods of Booth *et al*. (2006) to provide a well-resolved semblance response in later velocity analysis). Each common-source gather therefore contains 44 traces. Where the spatial sampling interval of Tx and Rx is the same, a CMP gather has half the number of traces of a common-source gather and the spatial sampling interval of those traces will be half that of the Tx and Rx move-up (Sheriff and Geldart, 1999). Consequently, the final spatial sample density of the multi-offset grid is $0.025 \times 0.05\,m^2$ and the fold-of-cover in CMP gathers is 22 (i.e. 2200%); this fold-of-cover implies that the horizontal stacking will increase signal-to-noise ratio by a factor of approximately 4.7. This survey took a further nine days to complete; again, an odometer wheel would have improved acquisition efficiency (e.g. the rapid multi-offset method described by Berard and Maillol, 2008) but we wished to ensure positional accuracy without interpolating traces. There was very little rainfall in the week before and during the three weeks of these acquisitions hence the moisture content and therefore the reflectivity of the subsurface is not expected to have changed.

Data processing and results

The GPR data from the spring 2006 survey were processed principally using Landmark Graphics

DOI: 10.1002/arp

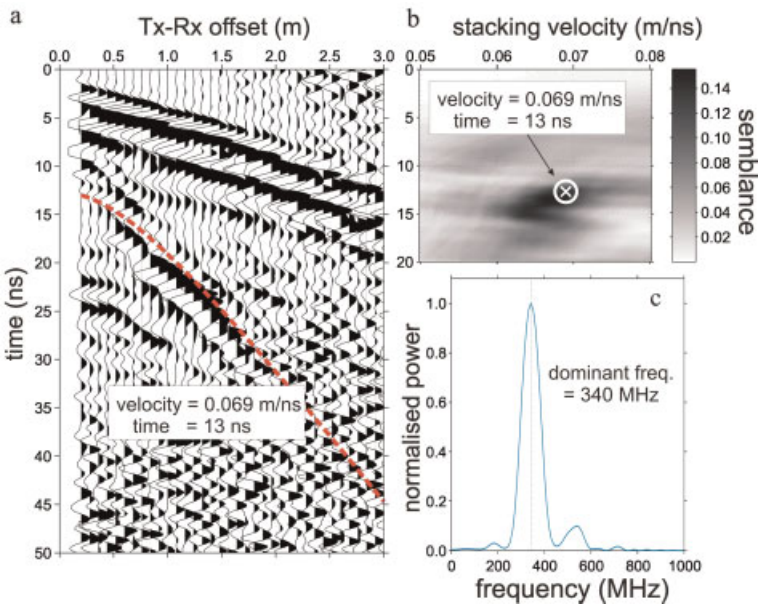

Figure 4. Representative CMP data acquired over the known position of a wall at the Groundwell ridge site, used to constrain spatial sampling interval for the spring 2006 GPR survey. a) CMP data, acquired with pulseEKKO1000 GPR system with 450 MHz antennas. Minimum offset 0.2 m, maximum offset 3.0 m, trace increment 0.04 m (note: for clarity, every other trace is shown). b) Semblance analysis of data presented in (a). A shallow reflection event is identified with stacking velocity and zero-offset two-way travel-time, respectively, of 0·069 and 13 ns; this semblance pick (annotated '⊗') is used to define the best-fit hyperbolae in (a). c) Power spectrum of the 0.2 m offset trace in (a), between 10–30 ns where useful signal amplitude is present. The dominant frequency of energy is 340 MHz. This frequency, and the near-surface velocity of 0.069 m/ns, were used in Equation 1 to obtain Δx_{max} of 0.05 m. This figure is available in colour online at www.interscience.wiley.com/journal/arp

Corporation *ProMAX*™; data were collated using Sandmeier *ReflexW*© and converted to SEG-Y format using the script SegyMAT (Hansen, 2004) in Mathworks *MATLAB*®. Processing flows for the common-offset and multi-offset grids are described in Figure 5. Note that in order to compare migration results with a conventional GPR acquisition, a grid of pseudo-three-dimensional common-offset data was extracted from the full-resolution three-dimensional common-offset grid at a sample density of $0.05 \times 0.50\,m^2$ (i.e. every tenth in-line). A more conservative bandpass filter is applied to the multi-offset data given that the dominant frequency of far-offset traces is lower than those at near-offset, due to signal attenuation. Energy is gained by compensating for the decay of the amplitude envelope of each trace; this operation is analogous to application of automatic gain control (AGC), but avoids the potential of AGC to introduce windowing artefacts to a dataset (Landmark Graphics Corporation, 2003). All grids were treated both with two-dimensional and three-dimensional Stolt migration algorithms (Stolt, 1978); two-dimensional migration was performed along the in-line direction of each grid. Multi-offset migration was performed using a semblance-derived velocity model that varies both spatially and temporally, with a Stolt stretch factor of 0.6; this velocity model was also used for earlier NMO corrections. The multi-offset velocity field does not extend across the entirety of the common-offset grid hence it cannot be reliably extrapolated. All common-offset migrations were therefore performed using a constant velocity of $0.069\,m\,ns^{-1}$ (using an appropriate Stolt stretch factor of 1.0), as would be conventionally performed for a common-offset acquisition in the absence of any multi-offset velocity field. Where a given processing step yields a dataset that is presented in Figures 6 and 7 (see later description and figures), that processing step is labelled accordingly. The computation of residual statics (Wiggins *et al.*, 1976), to compensate travel-time variability due to differential surface coupling, was deemed

DOI: 10.1002/arp

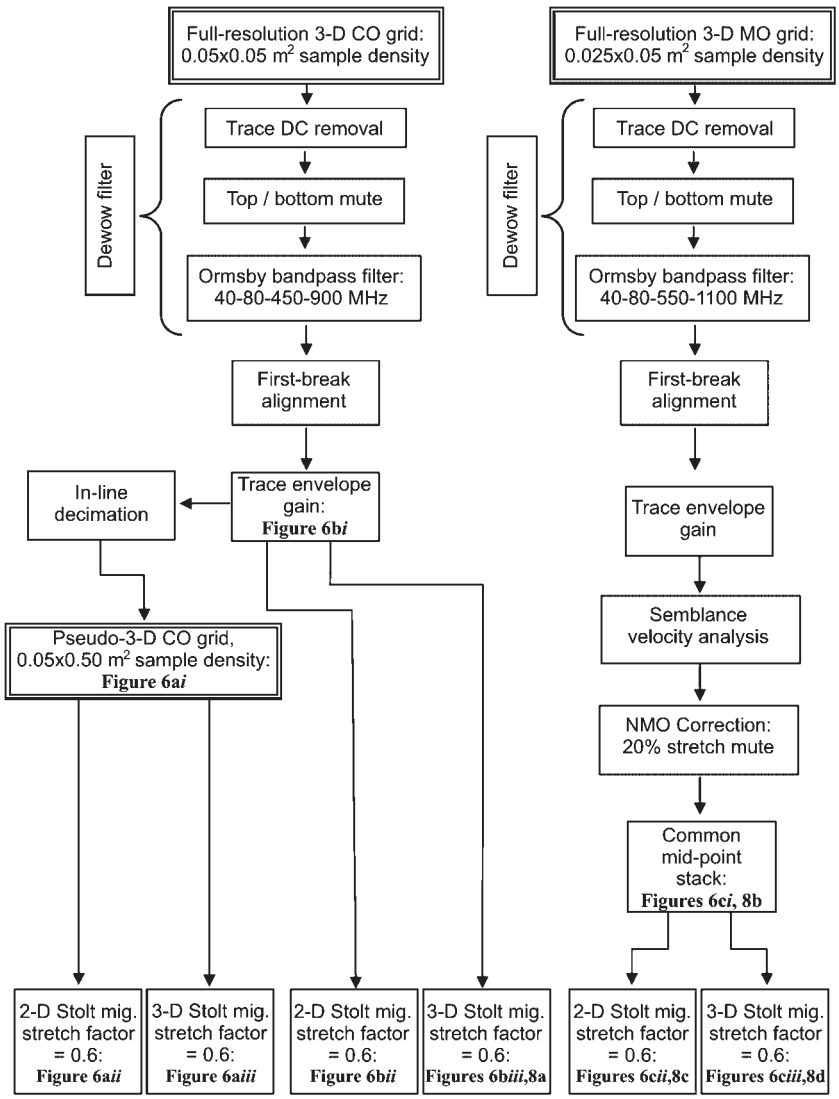

Figure 5. Processing flow for the common-offset and multi-offset data. After pre-processing, the full-resolution common-offset grid was decimated in the cross-line direction (i.e. every 10th in-line is extracted) to simulate a pseudo-three-dimensional common-offset acquisition. All datasets are treated with two-dimensional and three-dimensional Stolt migration algorithms; common-offset migration uses a constant velocity of 0.069 m/ns, multi-offset migration uses the velocity model derived from the semblance analysis. Where a process yields a dataset that is presented in Figures 6 and 8, that process is labelled accordingly.

unnecessary. Field observations suggested that the largest air gap beneath antennae was 0.05 m (due to microtopography and vegetation), implying a negligible modification to the travel time to target reflectors of +1%.

We should also consider the anisotropic radiation pattern of GPR antennae during data processing. In production of seismic surveys, the extensive use of source and receiver arrays introduces angular directivity to radiated amplitudes (e.g. Loveridge *et al*., 1984; Hustedt and Clark, 1998); in many cases, this directivity is not compensated for during processing and radiation is assumed isotropic (Ziolkowski *et al*., 1982). The radiation pattern from a GPR antenna is more complex than that of a seismic source, and comprises amplitude nulls at certain angles (e.g. Annan, 2005). Multi-channel processing

DOI: 10.1002/arp

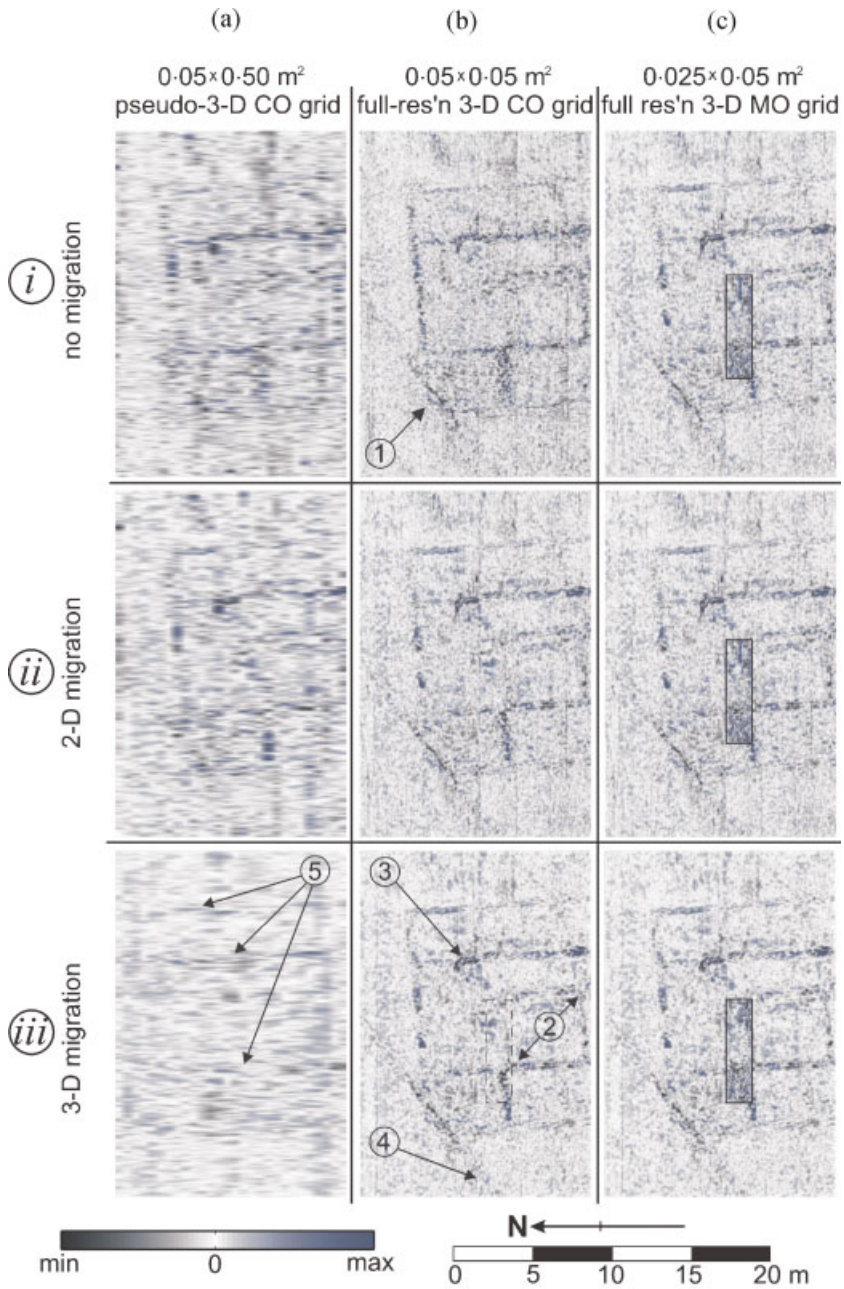

Figure 6. Time-slices from the spring 2006 GPR survey at Groundwell Ridge, extracted from TWT of 19 ns (0.66 m). Columns of this figure represent increasingly complex acquisition strategies; respectively, a, b and c refer to pseudo-three-dimensional common-offset (0.05×0.5 m^2), full-resolution three-dimensional common-offset (0.05×0.05 m^2) and full-resolution three-dimensional multi-offset (0.025×0.05 m^2, 2200% fold-of-cover) acquisitions. Rows of this figure represent increasingly complex migration strategies; respectively, ***i***, ***ii*** and ***iii*** refer to unmigrated, two-dimensional migrated (along in-lines) and three-dimensional migrated data. Annotations ①-⑤ are discussed in the main text.

DOI: 10.1002/arp

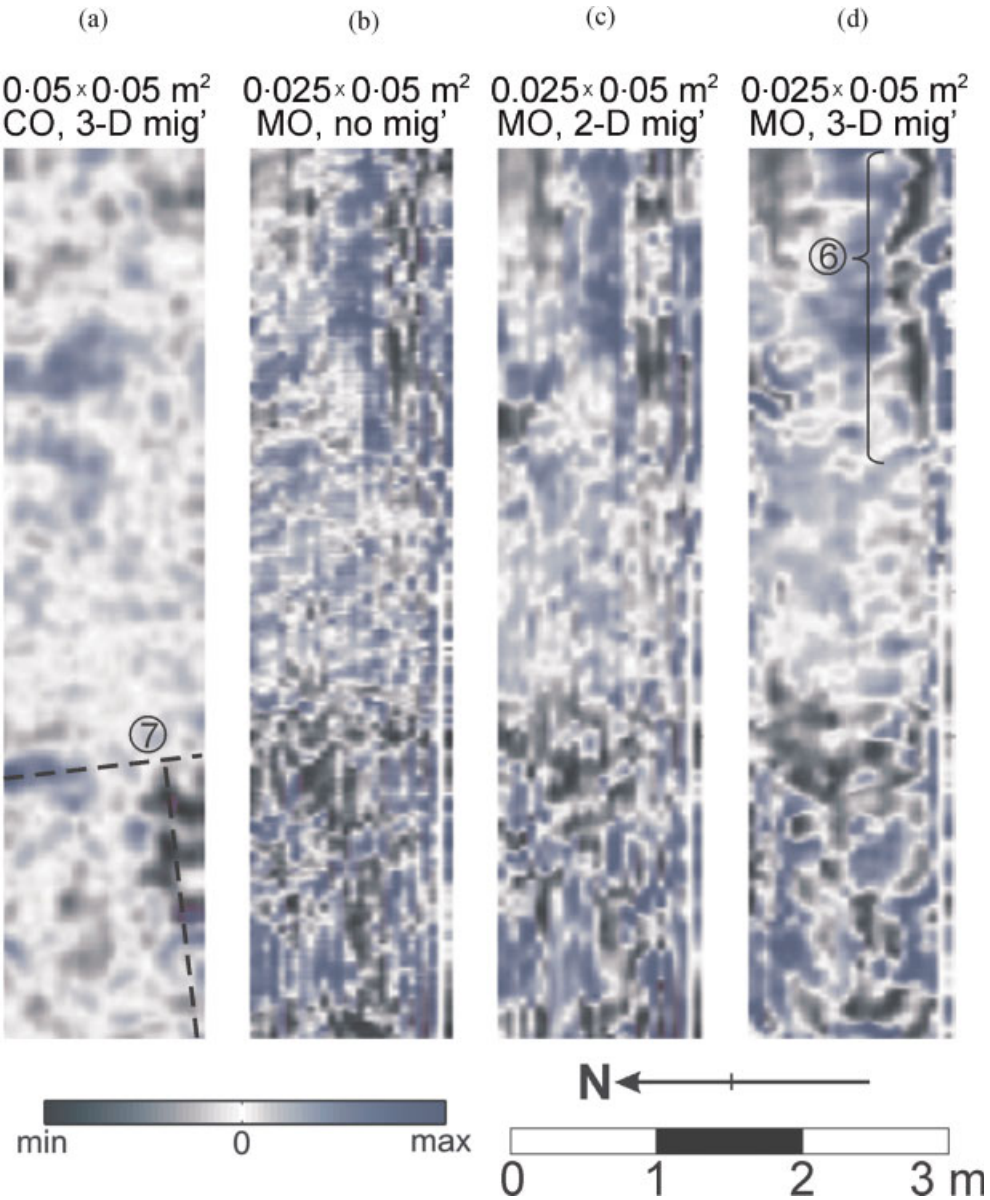

Figure 7. Enlargement of the multi-offset grids from Figure 6c, with synchronous common-offset data. a) Full-resolution, three-dimensional common-offset data extracted from Figure 6b*iii*. b) Unmigrated multi-offset data. c) two-dimensional migrated multi-offset data. d) three-dimensional migrated multi-offset data. Annotations ⑥ and ⑦ are discussed in the main text.

algorithms, such as migration and velocity analysis, may therefore require modification before an optimal processing strategy may be implemented for the GPR case. For velocity analyses, one improvement could be to include offset-weighting to the algorithm; such an approach is used by the seismic industry to compensate the effects of amplitude-versus-offset (AVO) on the reflection coefficient at an interface (e.g. Sarker *et al*., 2001; Swan, 2001). However, in this introductory investigation of a three-dimensional multi-offset processing

DOI: 10.1002/arp

strategy, we follow the example of standard seismic processing and assume a spherically symmetric radiation pattern.

Figure 6 shows time-slices of the Groundwell Ridge GPR data, from the 2006 survey. A conventional approach to time-slicing of GPR data involves calculating the analytic envelope of each trace, then averaging amplitudes within some fixed window length; the averaging process decreases the vertical resolution of the GPR time-slices, but such an approach has been shown to boost SNR (e.g. Goodman *et al.*, 1995). In this case, we wish to show the increase to SNR introduced by the three-dimensional migration and multi-offset algorithms while maintaining high vertical resolution in our time-slices. We therefore omit, in this figure, the calculation of the analytic envelope and present time-slices that have a thickness of one temporal sample. With the omission of the envelope, the polarity of traces is preserved hence averaging should not be conducting since amplitude cancellation may occur. Furthermore, the polarity of the GPR wavelet may yield useful information regarding either a change in the depth to a reflector or as a diagnostic of an effect of velocity pull-up (e.g. Leckebusch, 2007).

Each time-slice in Figure 6a is extracted from each data volume (i.e. each sample density and migration strategy) from TWTT of 19 ns, as for the image in Figure 2; with a velocity of $0.069\,\mathrm{m\,ns^{-1}}$, this corresponds to a depth of 0.66 m and a slice thickness of 0.003 m. Columns a, b and c of Figure 6 show data acquired with an increasingly complex acquisition strategy; 6a shows data from the $0.05 \times 0.5\,\mathrm{m}^2$ pseudo-three-dimensional common-offset grid, 6b from the $0.05 \times 0.05\,\mathrm{m}^2$ full-resolution three-dimensional common-offset grid and 6c shows the $0.025 \times 0.05\,\mathrm{m}^2$ multi-offset grid (where fold of cover exceeds 2000%) placed over the larger common-offset grid. Rows *i*, *ii* and *iii* show data processed with an increasingly complex migration strategy; 6*i* shows unmigrated data, 6*ii* shows two-dimensional migration of data along in-lines and 6*iii* shows full three-dimensional migration. As such, Figure 6a*i* (for example) refers to data extracted from the unmigrated pseudo-three-dimensional common-offset volume. For clarity, enlargements of the multi-offset grid and co-located data from the full-resolution three-dimensional common-offset grid are presented in Figure 7. It should be noted that the multi-offset time-slices, although synchronous with those from the common-offset volume, are not necessarily co-located in depth, since the spatially and temporally variant velocity model used for NMO correction was not extrapolated to the full extent of the common-offset grid.

The effect of different migration strategies on spatial resolution can be observed by comparing the images in columns a and b of Figures 6, from the pseudo- and full-resolution three-dimensional common-offset volumes. The outline and certain internal structures of the villa may be observed in both unmigrated time-slices (6a*i* and 6b*i*), together with the modern ferrous pipe; the image from the full-resolution three-dimensional common-offset survey is more interpretable although, without migration, this is simply because sample density is so high. However, note how it is possible to see the ferrous pipe actually cutting the northern wall (①). When two-dimensional migration is applied along the in-line direction (6a*ii* and 6b*ii*), resolution is somewhat improved for both data volumes. However, given the structural complexity of the target, certain responses may be migration artefacts since only anomalies which trend perpendicular to in-lines can be correctly migrated. This is particularly relevant for the image of the ferrous pipe since it trends at approximately 45° to the in-line direction. Only when three-dimensional migration is applied to the full-resolution three-dimensional common-offset volume can out-of-plane energy be migrated correctly; the spatial resolution in Figure 6b*iii* is superior to other time-slices, and we consider that the image contains fewer migration artefacts than Figure 6b*ii*. The spatial resolution of certain wall junctions is greatly improved (②), as is the definition of a high-amplitude feature along one of the interior walls (③); furthermore, the location of the pipe is more clearly defined away from the northern wall of the building (④). Three-dimensional migration of the pseudo-three-dimensional dataset greatly degrades image quality because this data volume is spatially aliased in the cross-line direction. However, note that features which trend

DOI: 10.1002/arp

perpendicular to the in-line direction are robustly migrated (⑤) given that in-line sampling satisfies full-resolution criteria.

Although three-dimensional migration of the full-resolution three-dimensional common-offset volume (6b*iii*) provides the best spatial resolution, the improvement when compared with the two-dimensional migrated volume is not generally significant. This implies that there is little out-of-plane energy at this site, in spite of the structural complexity. The high clay content suggests that the GPR wavelet will be rapidly attenuated, hence energy will not propagate far out of the plane of a survey line before being dissipated. Notice in Figure 4a that coherent signal energy does not persist beyond offsets greater than 1.5 m; out-of-plane energy will therefore only originate from a maximum horizontal distance of 0.75 m from the mid-point between the antennae. Consequently, diffraction hyperbolae do not exhibit long-offset diffraction tails, either in- or out-of-plane, hence the benefit of applying three-dimensional migration is somewhat reduced. The application of three-dimensional migration alone may therefore be better demonstrated at an archaeological site hosted in low-loss media (e.g. a target located in dry, sandy soil).

Multi-offset methods were used to boost signal amplitude over a low-SNR section of data, where interpretation was difficult in all common-offset datasets (i.e. considering both the 2002 and 2006 surveys). The dashed enclosure in Figure 6b*iii* shows the location of the multi-offset grid with respect to the three-dimensional migrated full-resolution dataset. When amplitudes from this section of data are viewed in isolation (Figure 7a) it is clear that SNR is very low indeed, and an interpretation of an interior wall can only be made with reference to surrounding structures as in Figure 6b*iii*. Figures 7b, c and d show unmigrated, two-dimensional migrated and three-dimensional migrated time-slices from the multi-offset dataset, respectively. All time-slices are again extracted from TWTT of 19 ns; recall, however, that data in Figure 7a are not necessarily co-located with those in 7b, 7c or 7d since a different velocity model is used for the common-offset and multi-offset processing. The presence of a wall therefore may be suggested in other time slices, even if this is not the case for Figure 7a. However, the velocity field derived from the multi-offset data is likely to be more accurate than the assumption of constant-velocity for the common-offset case, hence the content of the multi-offset time-slices is more representative of the subsurface at 19 ns TWTT.

Only when three-dimensional migration is applied to the dataset does coherent structure appear; a reflection is observed in Figure 7d, at the southern edge of the grid, trending east-west (marked ⑥). When the common-offset volume is overlain by the multi-offset time-slice (Figure 6c*iii*), the high-amplitude reflection fits well into the location of the orientation of the other walls. As such, we believe that the multi-offset method has boosted SNR such that the presence of an east–west trending interior wall can be suggested, although it is 2–3 m north of its originally interpreted position. We emphasize that this wall was only imaged using integrated full-resolution and multi-offset acquisition techniques; given that the wall cannot be seen in Figure 7b or 7c, the interpretation benefited both from boosted SNR and the application of three-dimensional migration.

Although the multi-offset method improved the image of one subsurface feature, we note that it degrades the interpretation of the wall junction to the east of the multi-offset grid (marked ⑦). This wall junction represents a particularly complex structure, hence the multi-offset dataset may benefit from application of a more sophisticated approach to migration (e.g., three-dimensional pre-stack time migration (Leparoux *et al*., 2001)).

The data in Figures 6 and 7 are not directly comparable to those from the 2002 acquisition since the time-slices we present are processed differently to those of Linford and Linford (2004). The latter are produced by considering the analytic envelope of traces, then averaging amplitudes over a number of temporal samples; in this way, the SNR in each image is boosted (e.g. Goodman *et al*., 1995). In order to compare the improvement to image quality that three-dimensional migration can yield, Figure 8 shows time-slices from the 2002 and 2006 acquisitions where an equivalent approach to time-slice processing is applied in each case; as in previous

DOI: 10.1002/arp

figures, the time-slice is extracted from a TWTT of 19 ns. Panels a and b show time-slices from the 2002 acquisition, c and d show data from the 2006 acquisition; note that, with the exception of the colour bar, panel c is exactly equivalent to Figure 6b*iii*.

In Figure 8a and c, the same approach to image processing is assumed as for the time-slices in

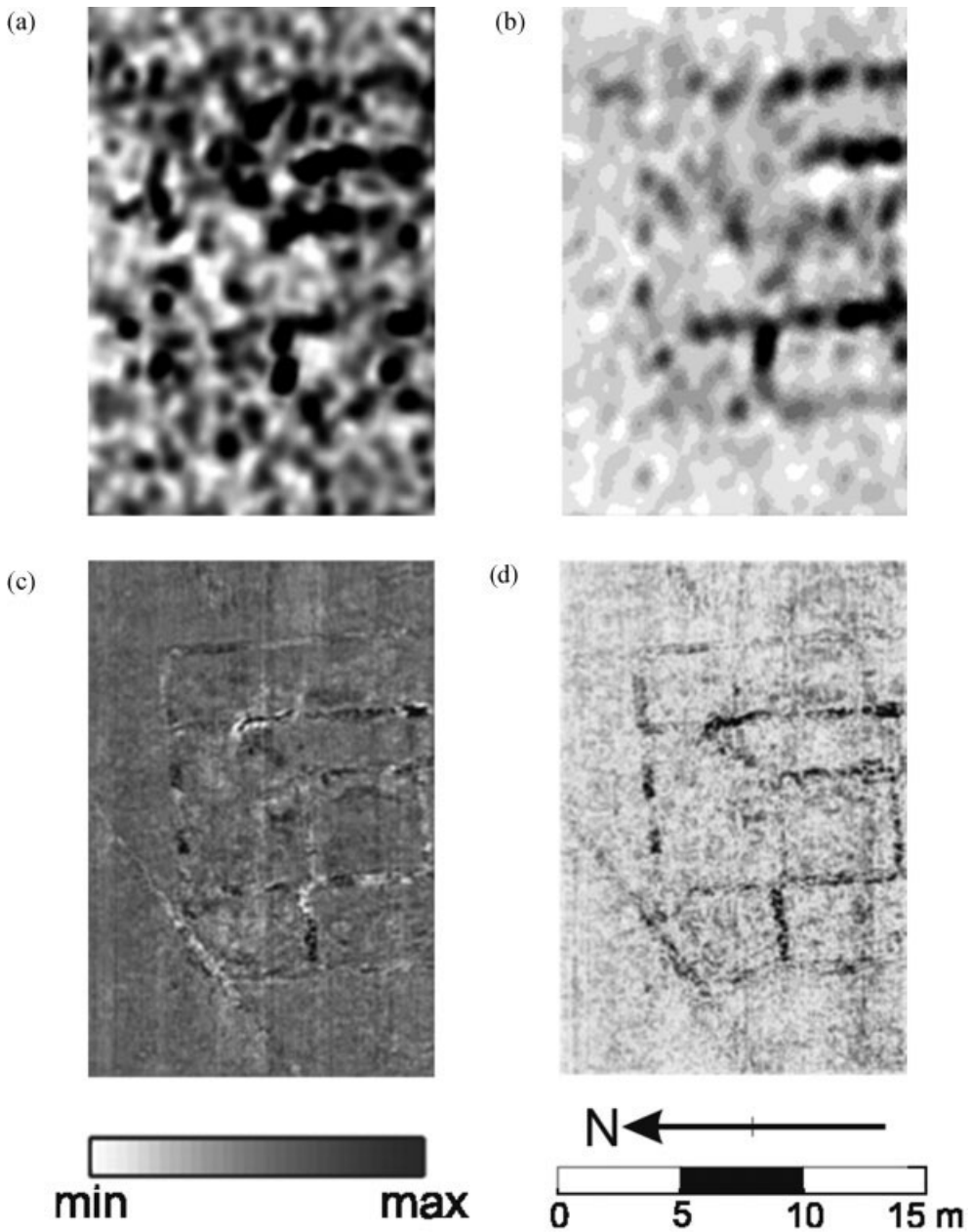

Figure 8. Time-slices from 19 ns TWTT, from the 2002 (a and b) and 2006 (c and d) GPR surveys. Time-slices in a and c are processed equivalently to those in Figures 6 and 7, with no consideration of the analytic envelope or temporal averaging. In b and d, a conventional approach to time-slicing is adopted; the analytic trace envelope is computed, and amplitudes are averaged over a 2 ns window (i.e. from 18 to 20 ns).

DOI: 10.1002/arp

Figure 6 (i.e. no analytic envelope or temporal averaging). In 8b and d, a conventional approach to processing is adopted; the analytic envelope of data is calculated, and amplitudes are averaged over a 2 ns window (in this case, from 18 to 20 ns). The consideration of averaged amplitudes greatly improves image quality for the 2002 acquisition; the archaeological target is much more visible in panel b than panel a. However, such marked improvement is not observed between panels c and d; image quality is not significantly enhanced where the time-slice is built from the analytic envelope of data. We therefore consider that the application of three-dimensional migration to this dataset is able to improve target visibility, without the need to decrease temporal resolution by considering the analytic envelope of traces. However, full-resolution and/or multi-offset acquisitions represent significant investments in field effort; we return to this point in later discussion.

Figure 9a shows the original interpretation (Linford and Linford, 2004) of the internal structure of the northern half of Groundwell Ridge villa, and a revised interpretation in Figure 9b, made by considering the whole volume of the common-offset and multi-offset datasets from the 2006 survey. Annotations denote walls which have been removed, modified from or added to the original interpretation. In each case, the dashed enclosure shows the extent of the common-offset grid.

The modified interpretation suggests that the eastern corridor extends as a single room along the entire length of the villa; two previously interpreted internal walls are now included among the classification in Figure 2 of 'other linear features' given that they can be traced beyond the eastern exterior wall. The western corridor remains largely unchanged, but its northern interior room now aligns better with the orientation of the rest of the villa. The centre of the villa still contains interior room divisions, except the central room is larger in dimension in the modified interpretation; an interior wall also spans the entire width between the flanking corridors.

Discussion

We have demonstrated that full-resolution three-dimensional and multi-offset GPR techniques have the potential to yield considerable

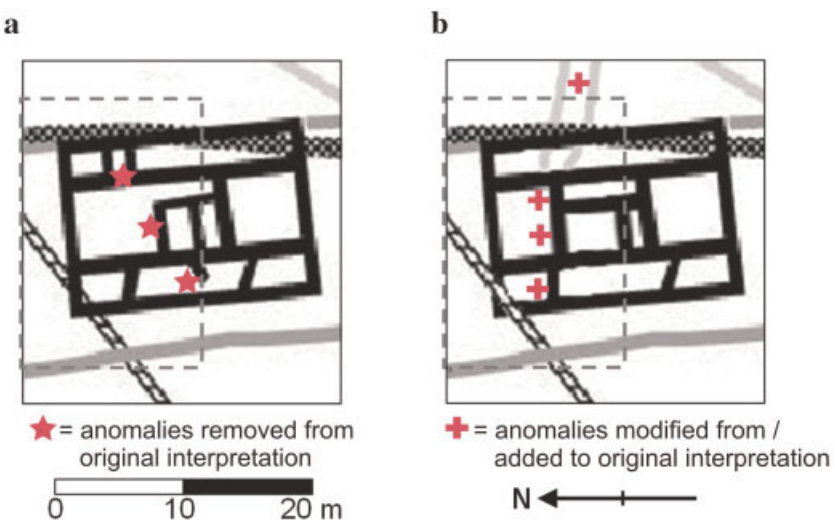

Figure 9. Modifications to the original interpretation of geophysical data from Groundwell Ridge, after analysis of the spring 2006 GPR data. Dashed enclosure shows the extent of the full-resolution, three-dimensional common-offset grid. a) Original interpretation, from Figure 2. The symbol ★ highlights anomalies that are removed in the new interpretation. b) Modified interpretation after analysis of integrated full-resolution common-offset and multi-offset data. The symbol ✚ highlights anomalies that are modified from, or added to, the original interpretation. This figure is available in colour online at www.interscience.wiley.com/journal/arp

DOI: 10.1002/arp

improvement to the spatial resolution and SNR of a subsurface image, compared to conventional pseudo-three-dimensional common-offset practice. This is particularly relevant to archaeological GPR surveying, where the management of archaeological remains favours non-invasive means of investigation and the interpretation of sites may therefore be increasingly based on geophysical survey data. However, it is not without good reason that three-dimensional and multi-offset methods are not more widespread throughout GPR surveying, as both require a significant increase in acquisition effort (e.g. Huisman *et al*. 2003; Berard and Maillol, 2008). Although our advanced GPR acquisition provided an improved image of the archaeological target, it is questionable whether that improvement is justified by a field campaign that took three weeks to cover an area of just 14 m × 21 m and was entirely reliant on the original EH data for accurate positioning over the remains of the villa. Furthermore, the full-resolution surveying of the whole 3.6 ha site in the 2002 survey would have been highly impractical particularly since conventional methods of producing time-slices allowed the target to be identified.

One method for improving the efficiency of full-resolution surveying would be to use a multi-channel GPR system, whereby multiple in-lines may be acquired simultaneously (e.g. Gustaffsson and Alkarp, 2007). However, the fixed offset between antennae in such systems implies that cross-line spacing cannot be easily modified for surveying at different locations. Until recently, the seismic industry minimized the expense of three-dimensional surveying by deliberately under-sampling the seismic wavefield in the cross-line direction; the sample density of cross-lines was typically up to five times sparser than required by full-resolution criteria (Sheriff and Geldart, 1999). Given that data processing is typically less expensive than acquisition, full-resolution criteria were recovered during data processing by application of trace interpolation algorithms (e.g. Kao *et al*., 1990; Spitz, 1991; Gülünay, 2003). The use of trace interpolation to improve sampling density has been superseded by the introduction of superior acquisition methods (e.g. as reviewed in Cambois, 2002), but the interpolation technique still has the potential to improve the efficiency of GPR surveying. If sparsely sampled pseudo-three-dimensional grids can be accurately upsampled to meet full-resolution criteria, the practicality of the three-dimensional survey method could be improved for common use.

Trace interpolation was applied to three pseudo-three-dimensional common-offset volumes, obtained by extracting in-lines from the unmigrated full-resolution three-dimensional volume. The spatial sampling density in each pseudo-three-dimensional volume was 0.05×0.10, 0.05×0.25 and $0.5 \times 0.50\,m^2$, requiring 2×, 5× and 10× upsampling to recover full-resolution sampling criteria. Although numerous, sophisticated, trace interpolation algorithms are available (e.g. Kao *et al*. 1990; Spitz, 1991; Nurul Kabir and Verschuur, 1995; Gülünay, 2003), for this trial we opted for a simple approach based on the coherency of energy across traces along specific dip trajectories (i.e. *beam-steering*) (Green *et al*., 1966; Rost and Thomas, 2002). A broad range of dip trajectories, up to ±20 ns per trace gap, was considered, with coherency assessed across five control traces. Interpolated data volumes were then migrated using a three-dimensional Stolt migration, again with a constant velocity of $0.069\,m\,ns^{-1}$ and stretch factor of 1.0.

Figure 10a-c show the 19 ns time-slice from trace interpolation of initial sample densities of 0.05×0.10, 0.05×0.25 and $0.05 \times 0.50\,m^2$; for comparison, Figures 10d and 10e are reproductions of Figures 6b*iii* and 6a*ii* (respectively, three-dimensional migration of full-resolution data, and conventional two-dimensional migration of pseudo-three-dimensional data). Where the degree of spatial aliasing is small, trace interpolation appears to perform well; time-slices support this, as the visual match between Figures 10a and 10d (i.e. a 2× upsampling) is very good. Where 10× upsampling was required, interpolated traces are a poor match for original traces given the poor match between Figures 10c and 10d. It could also be argued that the image in Figure 10e is superior to Figure 10c given that the latter contains interpolation artefacts (e.g. striping) in the cross-line direction. Where 5× upsampling was required, interpolated traces still appear to be close approximations to original

DOI: 10.1002/arp

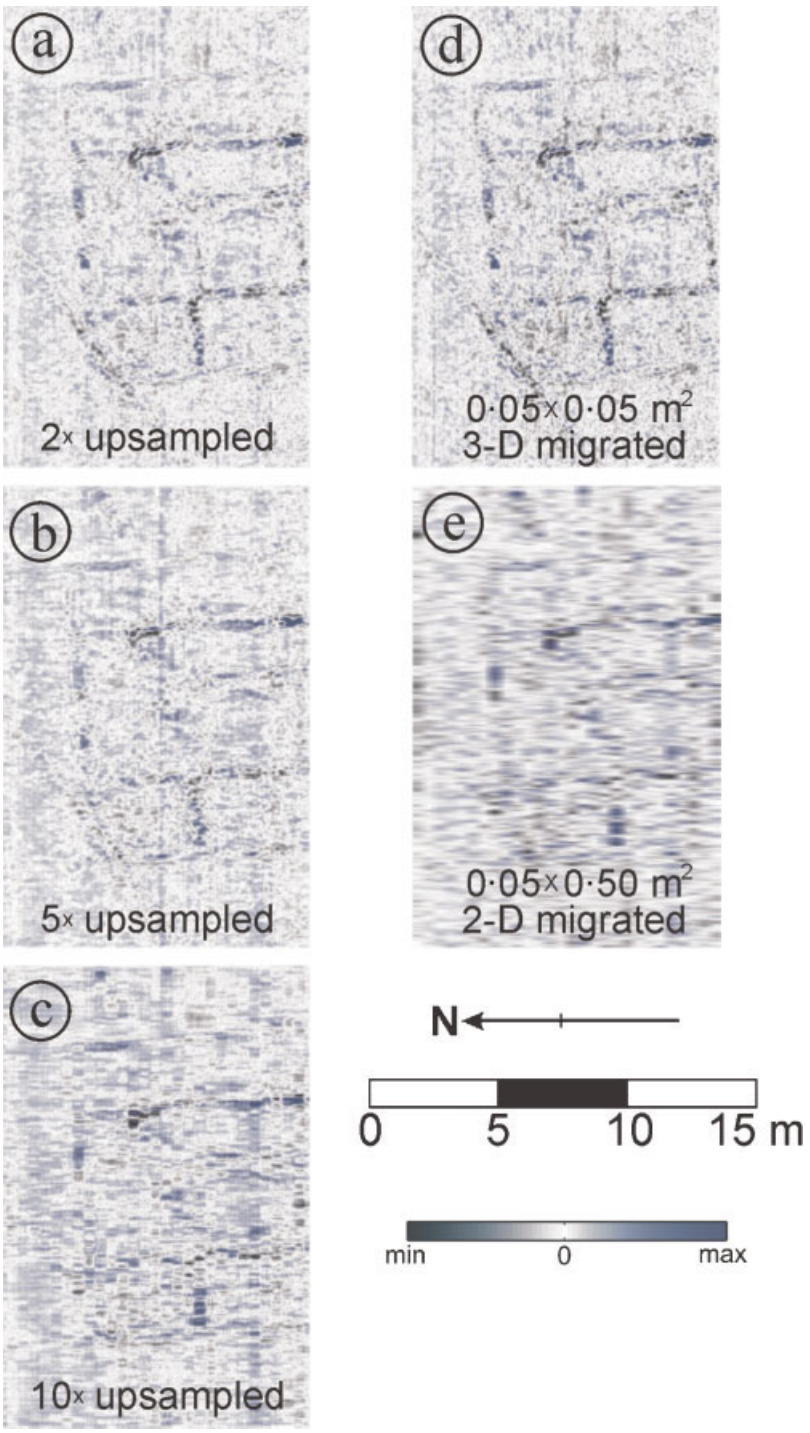

Figure 10. Investigation of trace-interpolation for the upsampling pseudo-three-dimensional data volumes to full-resolution three-dimensional sampling criteria (i.e. 0.05 × 0.05 m^2). All interpolations are performed using a beam-steering algorithm prior to application of three-dimensional migration. Time-slices, at TWTT of 19 ns, are extracted from three-dimensional migrated volumes where data are upsampled from initial sample densities of: a) 0.05 × 0.10 m^2, b) 0.05 × 0.25 m^2 and c) 0.05 × 0.50 m^2. For comparison, d) and e) show three-dimensional migrated full-resolution and two-dimensional migration pseudo-three-dimensional grids, respectively, as in Figures 6b*iii* and 6a*ii*.

DOI: 10.1002/arp

traces; the image of the target is highly comparable between Figures 10b and 10d.

The performance of the trace interpolation algorithm in Figure 10b is satisfying because it suggests that, just as in the seismic industry, full-resolution survey criteria can be relaxed. Results from our experiment at this site suggest that where a pseudo-three-dimensional grid is acquired with sample density of $0.05 \times 0.25\,m^2$, trace interpolation may be used to obtain a good approximation to a full-resolution grid. When the interpolated volume is three-dimensionally migrated, image quality will be comparable to that obtained from a full-resolution three-dimensional acquisition. If the in-lines in conventional pseudo-three-dimensional acquisition are separated by 0.5 m, surveying at a sample density of $0.05 \times 0.25\,m^2$ represents only a two-fold increase in acquisition effort for the significant improvement in image quality that trace interpolation and three-dimensional migration offers. We therefore suggest, for efficient full-resolution surveying, that the maximum separation between in-lines should be no greater than five times the value suggested by Equation 1. In this way, the compromise between the fieldwork effort, and the resulting image quality, of full-resolution three-dimensional GPR surveying can be minimized.

Currently, multi-offset acquisition is particularly inefficient and it is difficult to envisage significant improvement without considerable modification to GPR system design. Multi-channel GPR systems are becoming more available, but commercial examples are unsuitable for multi-offsets surveying as offset between antennae may not be easily customized. However, where an image of a low-SNR target is required, the multi-offsets method nonetheless provides the means of boosting amplitudes such that an improved subsurface interpretation can be obtained.

Conclusions

We have shown that use of advanced GPR acquisition and processing techniques can significantly improve the image of an archaeological target. Where structural complexity impedes interpretation, full-resolution survey methods can be applied such that three-dimensional migration methods are facilitated. If SNR in a dataset is poor, multi-offset techniques offer the capability to boost signal amplitudes. Where three-dimensional and multi-offset methods are combined, the potential improvement to imaging is significant, although extended processing may be required where structures are highly complex. Practical application of these techniques provided an improved image of an archaeological target, allowing a more robust interpretation to be made.

Acquisition criteria for such advanced surveys require considerable investment in survey effort, compared with conventional practice. In particular, with current GPR technology, there is little means to improve the efficiency of multi-offset surveying. However, criteria for acquisition of full-resolution data may be relaxed from their theoretical recommendations if a trace interpolation algorithm is used to upsample a pseudo-three-dimensional grid. In this way, a useful compromise is made between acquisition effort and image quality. We hope that full-resolution three-dimensional GPR surveys will be given more consideration for subsurface geophysical investigation.

Acknowledgements

This project was funded by an industrial CASE partnership between the Natural Environment Research Council and English Heritage (NER/S/A/2004/12333). Ground-penetrating radar equipment was obtained from the Geophysical Equipment Facility of the Natural Environment Research Council under loan number 816. We greatly appreciate the assistance in the field of Clare Little, Luke Jackson, Helena Sykes, Lucy Catt, Helen Freeman and Jared West. Andy Carter, Uri Schattner and Moshe Reshif provided useful advice during acquisition and processing. University of Leeds acknowledges provision of ProMAX™ by Landmark Graphics Corporation via the Landmark University Grant Program, Agreement 2004-COM-024982. We are grateful for the comments of two anonymous reviewers during the preparation of this manuscript.

DOI: 10.1002/arp

References

Annan AP. 2005. Ground-Penetrating Radar. C In *Near-Surface Geophysics*, Butler DK (ed.). Society of Exploration Geophysics: Tulsa, OK; 357–438.

Bano M, Pivot F, Marthelot J-M. 1999. Modelling and filtering of surface scattering in ground-penetrating radar waves. *First Break* **17**(6): 215–222.

Booth AD, Clark RA, Murray T. 2006. Semblance analyses for the design and interpretation of common mid-point GPR surveys. *Eleventh International Conference on Ground Penetrating Radar*, 19–22 June, Columbus, OH.

Berard BA, Maillol J-M. 2007. Multi-offset ground-penetrating data for improved imaging in areas of lateral complexity - applications at a Native American site. *Journal of Applied Geophysics* **62**: 167–177.

Berard BA, Maillol J-M. 2008. Common- and multi-offset ground penetrating radar study of a Roman villa, Tourega, Portugal. *Archaeological Prospection* **15**: 32–46.

Cambois G. 2002. Seismic acquisition: cheaper, better, faster... and safer. *The Leading Edge* **21**: 624.

Fisher E, McMechan GA, Annan AP. 1992. Acquisition and processing of wide-aperture ground-penetrating radar data. *Geophysics* **57**(3): 495–504.

Gaffney CF, Gater JA, Linford P, Gaffney VL, White R. 2000. Large-scale systematic fluxgate magnetometry at the Roman city of Wroxeter. *Archaeological Prospection* **7**: 81–99.

Gaffney VL, Patterson H, Piro S, Goodman D, Nishimura Y. 2004. Multimethodological approach to study and characterize Forum Novum (Vescovio, Italy). *Archaeological Prospection* **11**: 201–212.

Goodman D, Nishimura Y, Rogers JD. 1995. GPR time slices in archaeological prospection. *Archaeological Prospection* **2**: 85–89.

Grasmueck M, Weger R, Horstmeyer H. 2004. Full-resolution 3D GPR imaging for geoscience and archaeology. *Tenth International Conference on Ground Penetrating Radar*, 21–24 June, Delft.

Grasmueck M, Weger R, Horstmeyer H. 2005. Full-resolution GPR imaging. *Geophysics* **70**(1): K12–K19.

Green PE Jr, Kelly EJ Jr, Levin MJ. 1966. A comparison of seismic array processing methods. *Geophysical Journal of the Royal Astronomical Society* **11**: 67–84.

Gülünay N. 2003. Seismic trace interpolation in the Fourier transform domain. *Geophysics* **68**(1): 355–369.

Gustaffson J, Alkarp M. 2007. Array GPR investigation of the cathedral of Uppsala. *Near Surface Geophysics* **5**(3): 203–207.

Hansen TM. 2004. *SegyMAT v1.03*. Neils Bohr Institute for Astronomy, Physics and Geophysics, University of Copenhagen.

Huisman JA, Hubbard SS, Redman JD, Annan AP. 2003. Measuring soil water content with ground penetrating radar: a review. *Vadose Zone Journal* **2**(4): 476–491.

Hustedt B, Clark RA. 1998. Source/receiver array directivity effects on marine seismic attenuation measurements. *Geophysical Prospecting* **47**: 1105–1119.

Kao JC-S, Schneider WA, Whitman WW. 1990. Automated interpolation of two-dimensional seismic grids into three-dimensional data volume. *Geophysics* **55**(4): 433–442.

Landmark Graphics Corporation. 2003. *ProMAX™ 2D Manual, v.2003.12.1*. Landmark Graphics Corporation: Houston, TX.

Leckebusch J. 2000. Two- and three-dimensional ground-penetrating radar surveys across a Medieval choir: a case study in archaeology. *Archaeological Prospection* **7**: 189–200.

Leckebusch J. 2003. Ground-penetrating radar: a modern three-dimensional prospection method. *Archaeological Prospection* **10**: 213–240.

Leckebusch J. 2007. Short report: Pull-up/pull-down corrections for ground-penetrating radar data. *Archaeological Prospection* **14**: 142–145.

Leparoux D, Gibert D, Côte P. 2001. Application of prestack migration to multi-offset ground-penetrating radar (GPR) data. *Geophysical Prospecting* **49**: 374–386.

Leucci G. 2002. Ground-penetrating radar survey to map the location of buried structures beneath two churches. *Archaeological Prospection* **9**: 217–228.

Lindsey JP. 1989. The Fresnel zone and its interpretative significance. *The Leading Edge* **8**(33): 33–39.

Linford NT, Linford PK. 2004. Short Report: Ground penetrating radar survey over a Roman building at Groundwell Ridge, Blunsdon St Andrew, Swindon, UK. *Archaeological Prospection* **11**: 49–55.

Linford PK. 1999. *Abbey Mead, Groundwell Ridge, Blunsdon St. Andrew, Wiltshire: Report on Geophysical Survey, 1997*. Unpublished Report, Number 15/1999, Ancient Monuments Laboratory: London.

Linford PK, Martin L. 2002. *Groundwell Ridge, Blunsdon St. Andrew, Swindon: Report on Geophysical Survey, March-April 2002*. Unpublished Report, Number 44/2002, Centre for Archaeology: Portsmouth.

Loveridge MM, Parkes GE, Hatton L, Worthington MH. 1984. Effects of marine airgun source array directivity on seismic data and source signature deconvolution. *First Break* **2**: 16–22.

DOI: 10.1002/arp

Mayne WH. 1962. Common reflection point horizontal data stacking techniques. *Geophysics* **27**(2): 927–938.

Neidell NS, Taner MT. 1971. Semblance and other coherency measures for multichannel data. *Geophysics* **36**(3): 482–497.

Nurul Kabir MM, Verschuur DJ. 1995. Restoration of missing offsets by parabolic Radon transform. *Geophysical Prospecting* **43**(3): 347–368.

Olhoeft GR. 1996. Application of ground penetrating radar. *Sixth International Conference on Ground Penetrating Radar*, 30 September–3 October, Sendai, Japan.

Pipan M, Baradello L, Forte E, Prizzon A, Finetti I. 1999. 2-D and 3-D processing and interpretation of multi-fold ground penetrating radar data: A case history from an archaeological site. *Journal of Applied Geophysics* **41**: 271–292.

Pipan M, Forte E, Guangyou F, Karvells P, Dal Moro G, Sugan M. 2004. Multi-fold GPR study of shallow structure and stratigraphy of unconsolidated sediments and rocks. *Tenth International Conference on Ground Penetrating Radar*, 21–24 June, Delft.

Pipan M, Forte E, Sugan M, Dal Moro G, Gabrielli P, Finetti I. 2005. Integrated geophysical methods for the high-resolution study and characterization of low-contrast archaeological targets. *Proceedings of the 6th Archaeological Prospection Conference*, Rome, 14–17 September.

Pomfret J. 2006. Ground-penetrating radar profile spacing and orientation for subsurface resolution of linear features. *Archaeological Prospection* **13**: 151–153.

Ranieri G, Van Dommelen P, McLellan K, Deidda GP, Sharpe L, Trogu A. 2005. Synergical use of geophysical methods to reduce the archaeological risk in a complex area. *Proceedings of the 6th Archaeological Prospection Conference*, Rome, 14–17 September.

Rost S, Thomas C. 2002. Array seismology: methods and applications. *Reviews of Geophysics* **40**(3): 1–27.

Sambuelli L, Socco LV, Brecciaroli L. 1999. Acquisition and processing of electric, magnetic and GPR data on a Roman site (*Victimulae*, Salussola, Biella). *Journal of Applied Geophysics* **41**: 189–204.

Sarker D, Castagna JP, Larner K. 2001. AVO and velocity analysis. *Geophysics* **66**(4): 1284–1293.

Sheriff RE, Geldart LP. 1999. *Exploration Seismology*, 2nd edn. Cambridge University Press: Cambridge.

Soil Survey of England and Wales. 1983. *Soils of England and Wales, Sheet 5, South-West England, 1:250,000*. HMSO: London.

Spitz S. 1991. Seismic trace interpolation in the *F-X* domain. *Geophysics* **56**(6): 785–794.

Stolt RH. 1978. Migration by Fourier transform. *Geophysics* **43**(1): 23–48.

Swan HW. 2001. Velocities with amplitude variations with offset. *Geophysics* **66**(6): 1735–1743.

Whiting BM, McFarland DP, Hackenberger S. 2001. Three-dimensional GPR study of a prehistoric site in Barbados, West Indies. *Journal of Applied Geophysics* **47**: 217–226.

Wiggins RA, Larner KL, Wisecup RD. 1976. Residual statics analysis as a general linear inverse problem. *Geophysics* **41**(5): 922–938.

Wilson RJA. 2002. *A Guide to the Roman remains in Britain*. Constable: London.

Witten AJ, Levy TE, Adams RB, Won IJ. 2000. Geophysical surveys in the Jebel Hamrat Fidan, Jordan. *Geoarchaeology* **15**(2): 135–150.

Yilmaz O. 2001. Seismic Data Analysis: Processing, Inversion and Interpretation of Seismic Data. Society of Exploration Geophysicists: Tulsa, OK.

Ziolkowski A, Parkes G, Hatton L, Haugland T. 1982. The signature of an air gun array: computation from near-field measurements including interactions. *Geophysics* **47**(10): 1413–1421.

DOI: 10.1002/arp